*Desalination and Water Treatment*
www.deswater.com
doi: 10.1080/19443994.2014.902334

54 (2015) 2504–2515
May

Taylor & Francis
Taylor & Francis Group

# Enhancement of photocatalytic activity on salicylic acid by nonmetal-doped $TiO_2$ with solvothermal method

Huiqin Wang[a], Xiaolin Liu[b], Xinlin Liu[a], Qingfeng Guan[a], Pengwei Huo[c,*], Yongsheng Yan[c]

[a]*School of Material Science & Engineering, Jiangsu University, Zhenjiang 212013, P.R. China*
[b]*School of Biology and Chemical Engineering, Jiangsu University of Science and Technology, Zhenjiang 212003, P.R. China*
[c]*School of Chemistry & Chemical Engineering, Jiangsu University, Zhenjiang 212013, P.R. China, Tel. +86 511 8879 0187; Fax: +86 511 8879 1108; email: huopw1@163.com*

Received 16 October 2013; Accepted 27 February 2014

ABSTRACT

Nonmetal-doped $TiO_2$ nanoparticles have been prepared by the solvothermal method. The as-prepared photocatalysts have been characterized by X-ray diffraction, UV–vis diffuse reflectance spectra, Scanning electron microscope, Transmission electron microscopy, Specific surface area (BET) and X-ray photoelectron spectroscopy. The results indicate different atom radius and valence of the N, S and B atoms that cause the different doping ways, and it could form different lattice, which led to different surface area and pore volume of as-prepared photocatalysts. It is confirmed that S as $S^{6+}$ incorporate into the crystal lattice of the S–$TiO_2$, which may be the O–S–O–Ti–O linkages in the crystal lattice. It may be N and S as Ti–N–O or Ti–N–$O_2$ and $S^{2-}$ in the crystal lattice of the N&S co-doped $TiO_2$, respectively, which may be the S–Ti–N–O linkages in the crystal lattice. Photocatalytic activity was studied by degradation of salicylic acid under visible light. The degradation rate of salicylic acid reached 76.25% with N&S co-doped $TiO_2$ photocatalyst in 120 min, which is the highest of all the as-prepared photocatalysts. Furthermore, the experimental data of photocatalytic degradation well followed the Langmuir–Hinshelwood kinetics.

*Keywords:* Photocatalytic activity; Salicylic acid; Nonmetal doped; $TiO_2$; Solvothermal method

## 1. Introduction

Salicylic acid is a key additive in many skin-care ointments, creams, gels, and transdermal patches, and it is also widely applied in scientific experiments. However, salicylic acid is residual into the wastewater, such as sanitary wastewater, pharmaceutical wastewater, and is easy to sublimate and evaporate along with the steam [1]. Therefore, innovative technologies for disposal of salicylic acid sewage are required. Semiconductor photocatalysis, as one kind of advanced oxidation processes in air purification, water disinfection, and hazardous waste remediation, is the most promising technology [2]. Among most semiconductors, titanium dioxide ($TiO_2$), which possesses more advantages of strong oxidizing power of photoproduction holes, commercially available, nontoxic, high photostability, and redox selectivity, is one of the most popular and

*Corresponding author.

promising materials in photocatalytic application [2,3]. However, the photocatalytic efficiency of $TiO_2$ is low by its large intrinsic band gap energy (3.2 eV for anatase) and narrow photoresponse under visible light irradiation. In order to improve the photocatalytic efficiency of $TiO_2$, much effort has been devoted to surfaced and structured modification of $TiO_2$, such as doping with noble metal [4], transition metals [5], nonmetal elements C [6], B [7], N [8], F [9], S [10], and I [11], and sensitized by organic molecules [12]. Owing to the low-carrier-recombination centers and high thermal stability of nonmetal-doped $TiO_2$ nanostructures [13], investigators have been increasingly focused on the development of nonmetal-doped $TiO_2$ systems. Among nonmetal doped, the substitutional doping of S has been proved that S is incorporated as $S^{4+}$ cations and replaced Ti ions in $TiO_2$ [14,15]. However, researchers have also shown that the partially occupied impurity bands can still act as recombination centers in this kind of single-doping system [16].

Some recent reports describe the developing of a co-doped method for enhancing the performance of photocatalysts, for instance N&B co-doped [17,18] and N&S co-doped $TiO_2$ [19–21]. Wu et al. [17] reported that the N&B co-doped $TiO_2$ nanoparticles possessed much higher photocatalytic activity than the N single-doped $TiO_2$ nanoparticles, exhibiting better synergistic effect of the co-doping. Alexander et al. [18] found that the photocatalytic activities of B&N co-doped materials were similar to those with the same level of B-only doping. Sathish et al. [19] prepared co-doped $TiO_2$ by thermal decomposition of Ti-based metal complexes in vacuum and nitrogen followed by air annealing, and the N and S atoms in the $TiO_2$ lattice were clearly identified as in Ti–N–O and sulfate ($S^{6+}$). However, in some reports, all of N and S atoms were directly bonded to Ti in the parent compound which was prepared through the inorganic complex route and a systematic decomposition of the Ti-complex, which leads to the controlled removal of N and S to N, S–$TiO_2$ [20,21].

In this work, hydrothermal synthesis, which occurred in organic solvents environments, under the simultaneous application of heat and pressure, has been used to successfully prepare single-doped and co-doped $TiO_2$ with one step. The structural, optical, and surface properties of the as-prepared photocatalysts were systematically investigated by X-ray diffraction (XRD), X-ray photoelectron spectroscopy (XPS), scanning electron microscopy (SEM), transmission electron microscopy (TEM), specific surface area (BET), and UV–vis diffuse reflectance spectra (UV–vis DRS). The photocatalytic activity of as-prepared photocatalysts was evaluated by degradation of salicylic acid.

## 2. Experiments

### 2.1. Materials and characterization

Tetrabutyl titanate (Chemically Pure, CP), ethylene glycol (Analytical Reagent, AR), urea (Analytical Reagent, AR), thiourea (Analytical Reagent, AR), boric acid (Analytical Reagent, AR), salicylic acid (Analytical Reagent, AR), and ethanol (Analytical Reagent, AR) were all purchased from Shanghai Chemical Reagent Co., Ltd. and used as received. P25 was obtained from Degussa. Distilled water was used throughout this work.

The SEM images were examined by S-4800 SEM and equipped with an energy-dispersive spectra (EDS) detector (HITACHI, Japan). transmission electron microscopy (TEM) analyses were conducted with a Tecnai 12 electron microscope (PHILIPS, Holland). Specific surface areas were measured using a NOVA 2000e analytical system made by Quantachrome Corporation (USA). XRD technique was used to characterize the crystal structure. In this work, XRD patterns were obtained with a D8 ADVANCE X-ray diffractometer (Bruker AXS Company, Germany) equipped with Ni-filtrated Cu K$\alpha$ radiation (40 kV, 30 mA). The 2$\theta$ scanning angle range was 10–80° with a step of 0.04°/0.4 s. UV–vis DRS of photocatalyst was obtained for the dry-pressed disk samples using Specord 2450 spectrometer (Shimazu, Japan) equipped with the integrated sphere accessory for diffuse reflectance spectra, using $BaSO_4$ as the reflectance sample. XPS datum was recorded with a PHI5300 spectrometer using Al K$\alpha$ (12.5 kV) X-ray source.

### 2.2. Preparation of photocatalyst

The (N, S, and B) single-doped and co-doped $TiO_2$ photocatalysts have been synthesized by hydrothermal method. The processes were followed: 13.6 mL Ti$(OC_4H_9)_4$ was added to 33.5 mL ethylene glycol under magnetic stirring. The molar ratio of doping agents was fixed as 1:1 or 1:1:1. Then the solutions were mixed together. After that the mixture was stirred until the clarification. The clear solution was then placed in a clean Teflon-lined stainless steel autoclaves (100 mL). Then the thermal treatment was processed at 200°C for 24 h. Solvent heat treatment, due to ethylene glycol with tetrabutyl titanate and symmetric structure of titanium glycolate, compared to sol-gel and hydrothermal methods, is better to slow down the growth process in a moderate environment. After solvothermal reaction, shutting the power, it was cooled naturally to room temperature. The product was washed with distilled water and ethanol thrice. The washed product was dried at 80°C for 12 h. Finally, the product was heated

at 500 °C in 30 min and kept at 500 °C for 3 h in a muffle. At last, the prepared photocatalysts were signed as TB (Ti: B = 1:1), TN (Ti: N = 1:1), TS (Ti: S = 1:1), TBN (Ti: B: N = 1:1:1), TBS (Ti: B: S = 1:1:1), and TNS (Ti: N: S = 1:1:1), respectively.

### 2.3. Photocatalysis experiments

The photocatalytic degradation reaction of salicylic acid was carried out at 298 K in a homemade photocatalytic reactor under visible light. The photochemical reactor contained 0.1 g photocatalyst and 100 mL of salicylic acid solution of different concentrations. After 20 min in the dark, it reached adsorption balance, its initial absorbency was determined. The photocatalytic reaction was initiating with one 500 W xenon lamp (wavelength range 400–780 nm), which the light intensity was 80 mW/cm$^2$ at a distance of 10 cm from the center of the lamp. The samples were conducted in 20-min interval under the conditions, which the reaction time was 100 min. And the residual amount of salicylic acid in the aqueous phase was measured using UV–vis spectrophotometer at 296 nm. The photocatalytic degradation rate (DR) was calculated by the followed equation.

$$DR = (1 - A_i/A_0) \times 100\% \quad (1)$$

where $A_0$ is the initial absorbency of salicylic acid solution and $A_i$ is the absorbency of reaction solution.

## 3. Results and discussion

### 3.1. SEM, TEM and EDS

Fig. 1 shows the microcosmic images of TS (a) and TNS (b) photocatalysts, it can be found that there are very similar particles. The morphology displayed rice-grains shape. The length of rice-grains particles is about size of 40–50 μm. The surfaces of the rice-grains particles are relatively smooth but anomalous. Fig. 2 shows the TEM morphology of the nanostructured crystalline TN and TNS. The TN and TNS are piled up by the highly intense uniform crystal. And the images of TN and TNS at high magnification show many randomly oriented nanocrystallites with sizes 20–30 nm and 10–15 nm, respectively. Fig. 3 shows the quantitative results for TS and TNS photocatalysts. As shown in Fig. 3, the element of S was determined in S–$TiO_2$ and N&S elements in N–S–$TiO_2$. And we can find the S contents of TNS photocatalyst are less than TS. Due to its larger ionic radius, successful insertion of sulfur into the $TiO_2$ lattice is far more difficult to achieve than nitrogen [22]. However, it has little effect on the morphology of TS and TNS photocatalysts. Maybe N and S elements insert into the internal lattice of $TiO_2$.

### 3.2. BET

The nitrogen adsorption–desorption isotherms results for the photocatalysts of TN and TNS were shown in Fig. 4. The isotherms should be attributed to the typical IV, which belonged characteristic of well-developed mesoporous materials. And the specific surface area values were calculated using datum of liquid nitrogen physisorption experiments with the Brunauer–Emmett–Teller (BET) method. The BET surface area of TN and TNS is 97.82 and 140.72 m$^2$/g, respectively. And the pore volume of TN and TNS could reach 0.10 and 0.16 cm$^3$/g, respectively. Fig. 5 shows the pore size distribution of TN and TNS. It can be calculated that BJH adsorption average pore

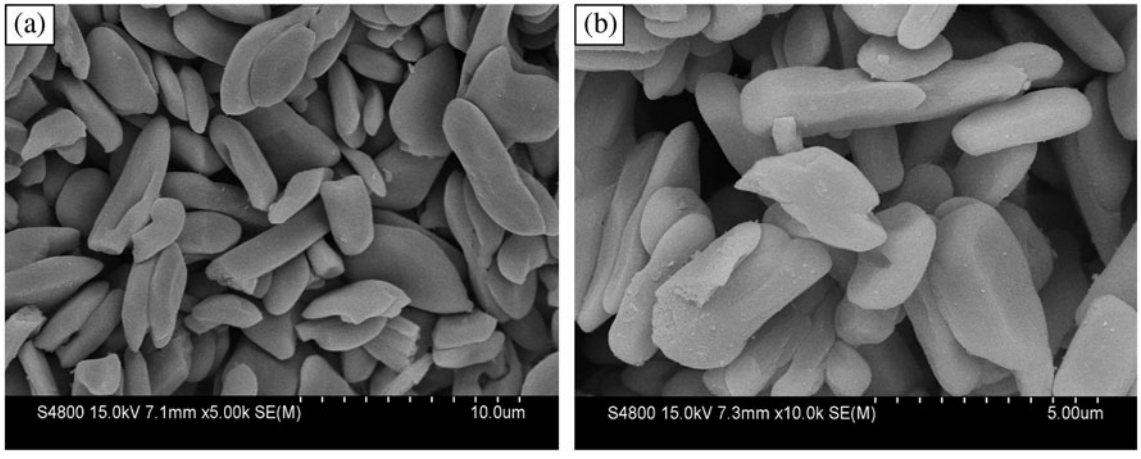


Fig. 1. The SEM images of photocataysts (a) TS and (b) TNS.

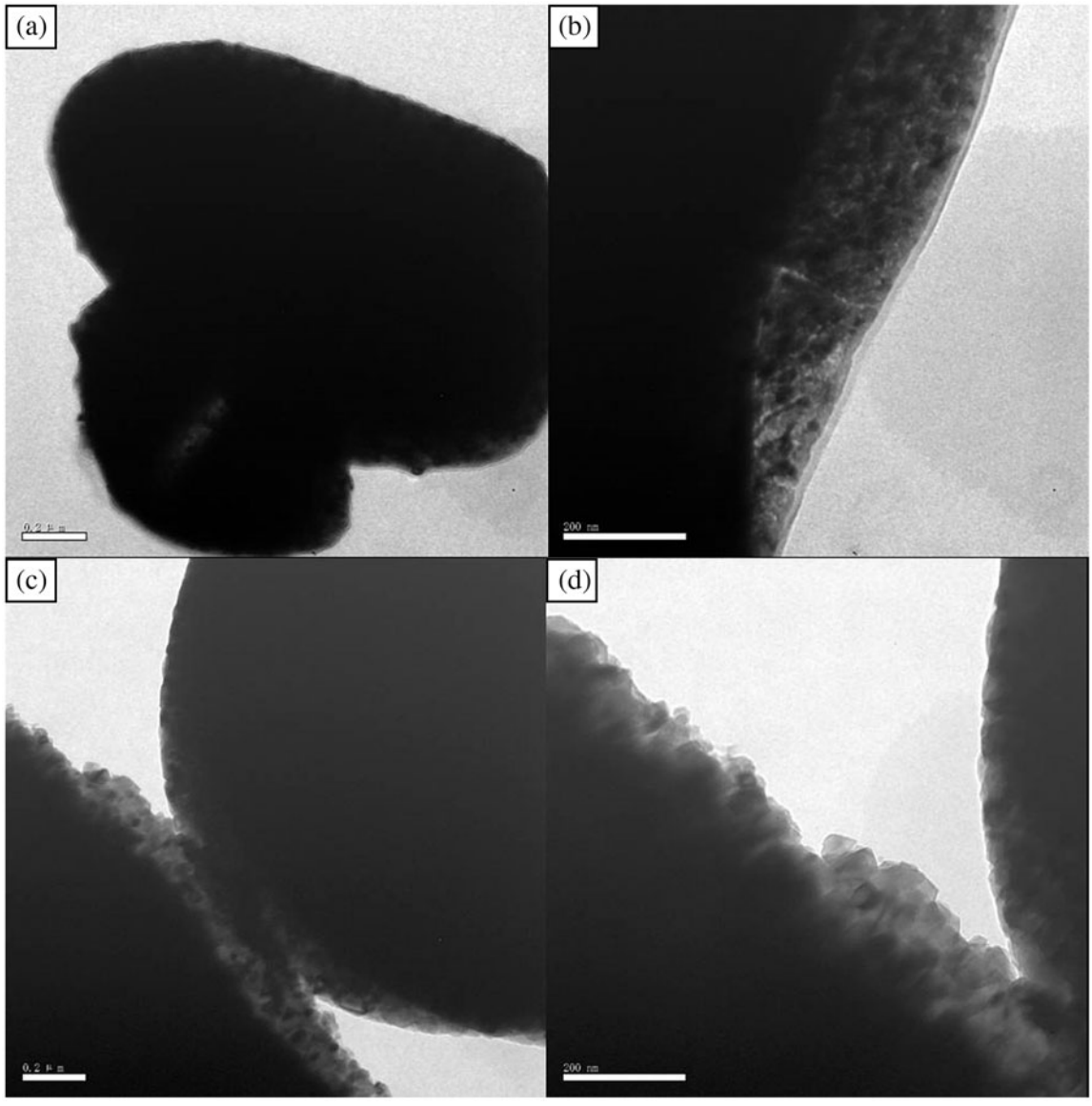


Fig. 2. The TEM images of photocataysts (a,b) TS and (c,d) TNS.

diameter of TN and TNS is 34.2 and 43.2 nm, respectively. With a relatively narrow pore size distribution, range from 10 to 50 nm, which almost the same as that observed from the TEM images. The smaller pore size may be attributed to the smaller micelle of ethylene glycol in the steam during the evaporation self-assembling solvothermal.

### 3.3. XRD

Fig. 6 shows the XRD patterns of different as-prepared photocatalysts. It can be found that the samples of co-doped and single-doped $TiO_2$ possess the same five characteristic sharp peaks at $2\theta = 25.38$, 37.66, 48.02, 53.98, and 62.7 correspond to (1 0 1), (0 0 4), (2 0 0), (1 0 5), (2 1 1) and (2 0 4) planes of anatase $TiO_2$ (JCPDS card no. 83-2243), respectively. For the co-doped and single-doped $TiO_2$, no featured peaks of rutile $TiO_2$ are observed. In addition, there are no featured peaks of nonmetal elements, which manifested that nonmetal element is maybe highly dispersed on $TiO_2$, or XRD is not sensitive enough to detect such minor changes for $TiO_2$. From the Scherrer formula [23], the average sizes of crystalline particles of the TNS, TBS, TBN, TS, TB, TN and $TiO_2$ could be calculated to be of 12.21, 17.66, 23.94, 32.44, 37.41, 36.27 and

(a)

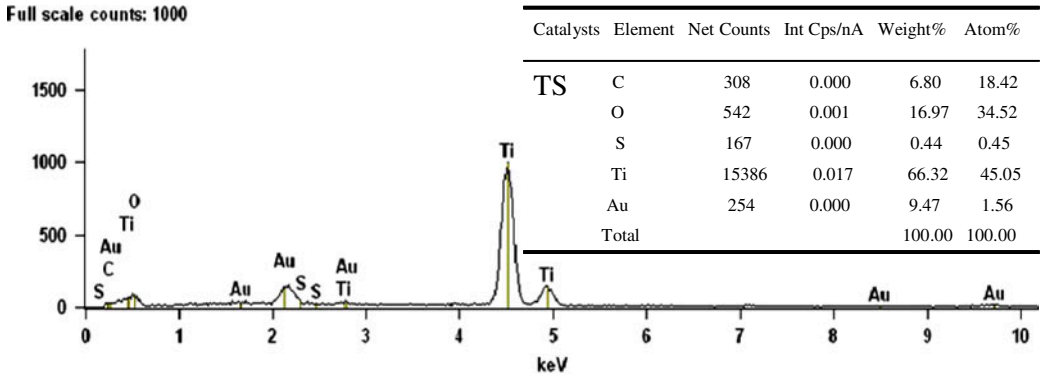


| Catalysts | Element | Net Counts | Int Cps/nA | Weight% | Atom% |
|---|---|---|---|---|---|
| TS | C | 308 | 0.000 | 6.80 | 18.42 |
| | O | 542 | 0.001 | 16.97 | 34.52 |
| | S | 167 | 0.000 | 0.44 | 0.45 |
| | Ti | 15386 | 0.017 | 66.32 | 45.05 |
| | Au | 254 | 0.000 | 9.47 | 1.56 |
| | Total | | | 100.00 | 100.00 |

(b)

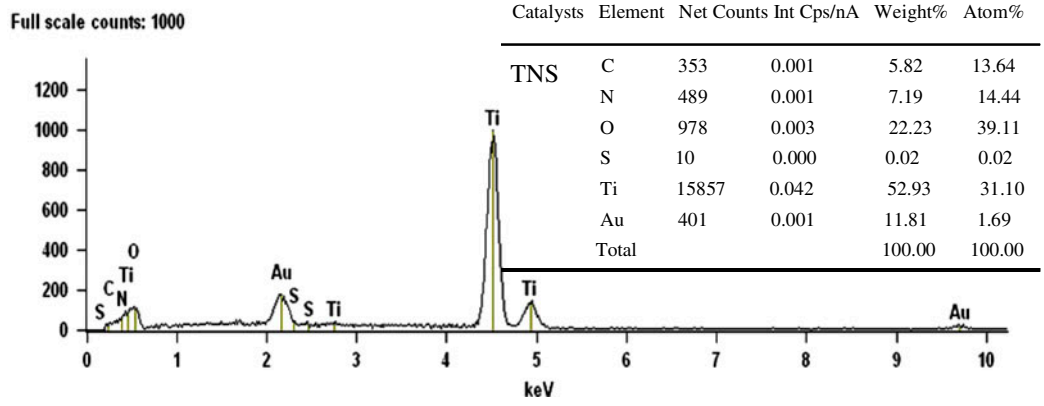


| Catalysts | Element | Net Counts | Int Cps/nA | Weight% | Atom% |
|---|---|---|---|---|---|
| TNS | C | 353 | 0.001 | 5.82 | 13.64 |
| | N | 489 | 0.001 | 7.19 | 14.44 |
| | O | 978 | 0.003 | 22.23 | 39.11 |
| | S | 10 | 0.000 | 0.02 | 0.02 |
| | Ti | 15857 | 0.042 | 52.93 | 31.10 |
| | Au | 401 | 0.001 | 11.81 | 1.69 |
| | Total | | | 100.00 | 100.00 |

Fig. 3. The EDS of as-prepared photocatalysts and inset of quantitative results for (a) TS and (b) TNS.

29.88 nm, respectively. The average sizes of the crystalline particles in the co-doped $TiO_2$ are smaller than that of the single-doped $TiO_2$ and pure $TiO_2$, illustrating that co-doped $TiO_2$ would reduce the growth of the $TiO_2$ crystals.

### 3.4. UV–vis DRS

To test the effect of single-doped and co-doped $TiO_2$ on the optical property, the UV–vis DRS are presented in Fig. 7. As shown in Fig. 7, it can be clearly found the single-doped and co-doped $TiO_2$ are obviously showed red-shifted. Especially, the adsorptions of TNS and TS are the highest among the co-doped and single-doped $TiO_2$ photocatalysts under visible light range, respectively. The band gap can be estimated by using $E = 1{,}240/\lambda$, which $E$ is the band gap energy and $\lambda$ is the wavelength of the absorption edge. So the values of TNS, TBS, TS, TBN, TB and TN were estimated to be of 2.75, 2.80, 2.84, 2.88, 2.90 and 2.94 eV, respectively. Therefore the adsorption of TNS is the highest of all the photocatalysts under visible light range. But, we can find that not all co-doped $TiO_2$ is higher adsorption than single-doped $TiO_2$ under visible light range.

### 3.5. XPS

The atom% content in both TN and TNS is summarized in Table 1. Undoubtedly, there is a difference in O and Ti atom% content in both TS and TNS. Such changes in atom% surface composition may indicate the redistribution or even a damage of a protective layer [24]. To determine how sulfur and nitrogen atoms incorporate in the crystalline lattice of $TiO_2$, the XPS spectra of TS and TNS photocatalysts nanoparticles are presented in Fig. 8. Fig. 8(b) and (f) shows the XPS spectrum of Ti 2p with TS and TNS photocatayst, two peaks of all the XPS spectrums are assigned to the Ti 2p1 (high binding energy) and Ti 2p3 (low binding energy) status in TN and TNS photocatalysts, respectively. The peaks of E (Ti 2p1) and E (Ti 2p3) are 464.33 eV (b), 464.45 eV (f), 458.78 eV (b) and 458.85 eV (f), respectively, which belong to $Ti^{4+}$ [25]. All peaks of the

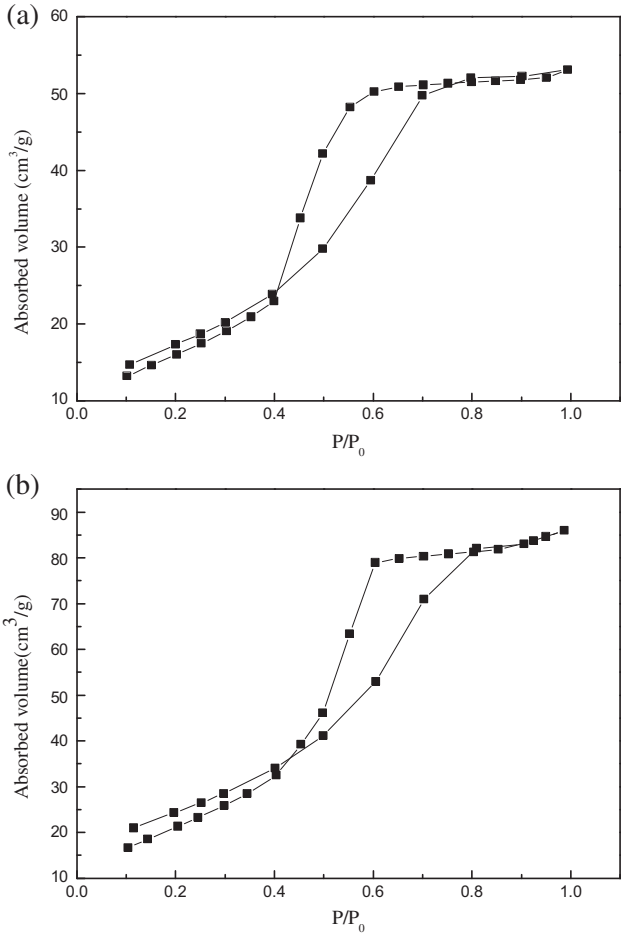


Fig. 4. Nitrogen adsorption–desorption isotherms. (a) TN and (b) TNS.

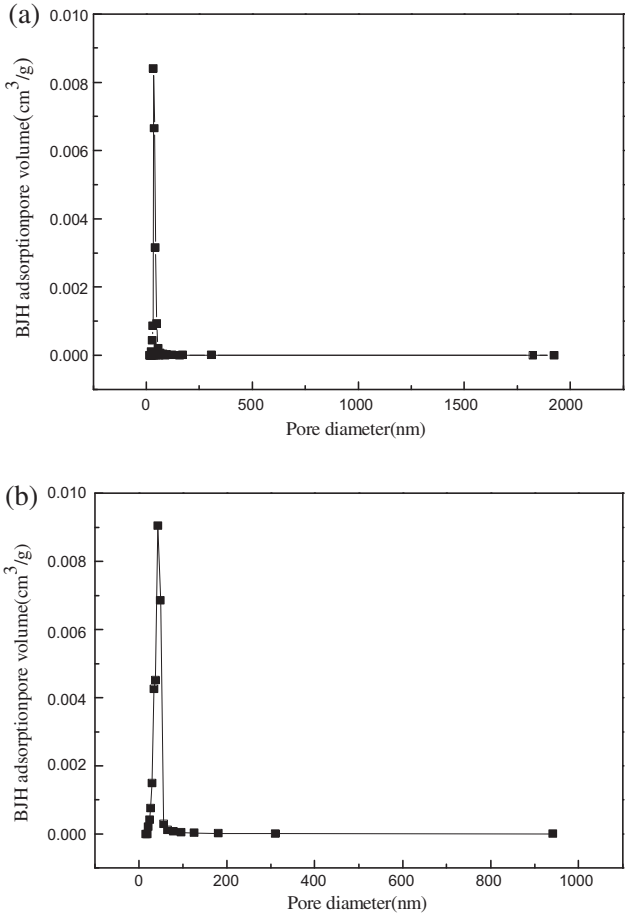


Fig. 5. The pore size distribution curves of (a) TN and (b) TNS.

single-doped and co-doped $TiO_2$ photocatasysts shift high energy compare to the pure $TiO_2$. And the energy of co-doped $TiO_2$ (TNS) is higher than single-doped $TiO_2$. And that the E (O 1s) is 530.69 eV (c) and 530.79 eV (g), which belong to the O–Ti–O lattice oxygen of TS and TNS photocatalysts. It indicates that the bond is stable. It is found from Fig. 8(d) that the S 2p of TS photocatalyst peak is located at 168.24 eV, which indicated that S is successfully incorporated into the $TiO_2$. There are no other S 2p features because of sulfide ($S^{2-}$ at ≤162 eV), elemental S as in TS ligands or parent complex (S at 164.0 eV) or sulfite ($S^{4+}$ at 166–167 eV) is observed from BE Lookup Table for Signals from Elements and Common Chemical Species. We deem the above sulfate feature in $S^{6+}$ oxidation to one or more of the following features in the diminishing order (sulfate as in titanium oxysulfate, sulfate at surfaces, interfaces and at grain boundaries or sulfate in the interstitial position of $TiO_2$) [19]. Of course, there are may be that sulfur interacts with nearby oxygen atoms in the anatase lattice [16]. Fig. 8(h) and (i) show the N 1s and S 2p core level feature from TNS photocatalyst. Fig. 8(h) and (i) indicate that the N 1s and S 2p of the TNS photocatalyst peak are located at 163.39 and 399.18 eV, which indicate that N and S are successfully incorporated into the $TiO_2$. As the interaction of N and S element, the form of S doped $TiO_2$ is changed. The doped N with the binding energy of 399.18 eV can be assigned to the Ti–N–O or Ti–$NO_2$ linkages [26]. Because of the impact of the N element and some deviation, the doped S with the binding energy is higher. Therefore, it can be inferred that S may be as $S^{2-}$ replaced O in the crystal lattice of the N&S co-doped $TiO_2$. Surface atom% composition shown in Table 1 shows a decrease in Ti% content in TS and TNS from 19.82% to 18.42%, proving that chemical re-distribution in lattice. And O–Ti content decreased 78.38% to 75.85%. In addition, the percentage of titanium element of TS photocatalyst is lower than pure $TiO_2$ from EDS. It indicates that some other effective positions of Ti are replaced by S in the crystal lattice of

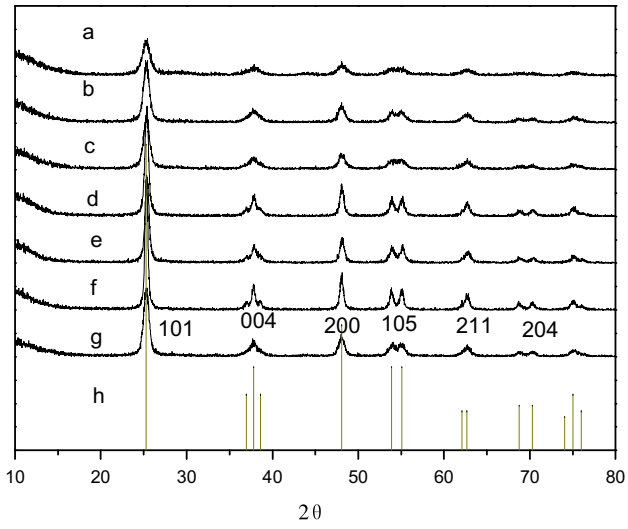


Fig. 6. XRD patterns of different samples (a) TNS, (b) TBS, (c) TBN, (d) TS, (e) TB, (f) TN, (g) $TiO_2$, (h) and standard spectra of anatase $TiO_2$.

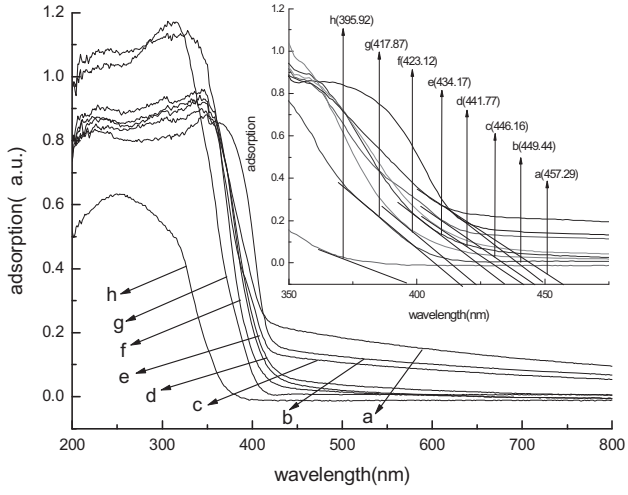


Fig. 7. The UV–vis DRS spectrum of different photocatalysts (a) TNS, (b) TBS, (c) TS, (d) TBN, (e) TB, (f) TN, (g) P25, and (h) $TiO_2$.

the TS photocatalyst. It may be the O–S–O–Ti–O linkages in the crystal lattice of the TS photocatalyst. However, the S content in TS and TNS decreased from 1.80 to 0.55%, which also proved from EDS. Therefore, it may be the S–Ti–N–O linkages in the crystal lattice of the TS photocatalyst.

### 3.6. Photocatalytic activity

The photocatalytic activity of the different photocatalysts was evaluated by degradation salicylic acid solution under visible light. As shown in Fig. 9, The rate of adsorption was rapid in the initial minutes of solution-adsorbent contact and it reached the equilibrium status after 10 min. the co-doped TNS shows better photocatalytic activity than the other photocataysts under visible light irradiation. About 76.25, 69.42, 66.80, 59.95, 55.40, 50.18, 48.58 and 30.77% salicylic acid are degraded in the presence of TNS, TBS, TS, TNB, TB, TN, P25 and $TiO_2$, respectively. Obviously, the TNS has the highest photocatalytic activity, it can be also found that the degradation rates of salicylic acid with TNS and TS are the highest between co-doped and single-doped $TiO_2$ under visible light range, respectively. And it can be clearly found that co-doped $TiO_2$ (TNS) shows better photocatalytic activity than single-doped $TiO_2$ (TN or TS). The result is obviously accorded with the analysis of UV–vis DRS. Co-doping $TiO_2$, owing to synergistic effect, may effectively promote the separation of photogenerated charge carriers, which can improve the photocatalytic activity. However, not all co-doped $TiO_2$ show better photocatalytic activity than all single-doped $TiO_2$. There are different atom radius and valence of the N, S and B atoms, which cause the different doping ways that there are substitutions and void doped for different atoms. It can be formed different lattice systems, which lead to different surface area and pore volume. Therefore, it possesses different photocatalytic activity for co-doped $TiO_2$ and single-doped $TiO_2$. Due to a large surface area and pore volume of TNS photocatalyst, indicating that the co-doped photocatalyst possesses more activated sites on the surface of photocatalyst, and it is better for adsorption of the salicylic acid onto the photocatalysts. Therefore, the more adsorption of salicylic acid is obtained, the higher degradation rate is showed under the same conditions. In addition, the large surface of the photocatalyst is not only offered more reaction sites, but also it is conducive to the photo capture and electron transfer, and it could generate enough activated groups for photo

Table 1
Atom % surface composition of TN and TNS (standard deviation is presented in the brackets)

| Catalysts | Element | Atom% |
|---|---|---|
| TN | S | 1.80 (0.1) |
| | O | 78.38 (0.7) |
| | Ti | 19.82 (2.1) |
| TNS | N | 5.19 (0.2) |
| | S | 0.55 (0.1) |
| | O | 75.85 (0.5) |
| | Ti | 18.42 (2.1) |

degradation which lead a better activity [27]. Furthermore, formation of large open pore on the surface of TNS photocatalyst may also be another important reason to enhance photocatalytic activity. Because such a large open pore is beneficial to exposure of more TNS crystallites to the solid–liquid interface and may also facilitate salicylic acid transport to the active sites [28]. And because of the intense recombination caused by the N and S doping of TNS, the new band gap status was created by the doping which indeed improve the photoresponse for visible light. And it is narrow band gap for TNS photocatalyst. Therefore the electron transport in the conduction band of TNS photocatalyst is fast. As shown in Fig. 10, increasing concentration of salicylic acid, the degradation rate of the photocatalysts is lower. However, the amount of degradation salicylic acid does not decrease with increased the amount of salicylic acid. And the TNS photocatalyst has a limited number of actives sites, which becomes saturated at a certain concentration. And the low concentration of salicylic acid can maintain a sustainable and stable to photocatalytic activity, which may avid deactivation of catalyst. Consequently, the concentration of the salicylic acid is important to the TNS photocatalytic activity.

In order to investigate the photodegradation dynamics process of salicylic acid with the photocatalyst of TNS. From Fig. 11, the first-order kinetic the entire linear regression coefficient ($R^2$) is greater than the second-order kinetic. Therefore photocatalytic degradation of salicylic acid obeyed first-order kinetic. The rate constant value of 10 mg/L salicylic acid was

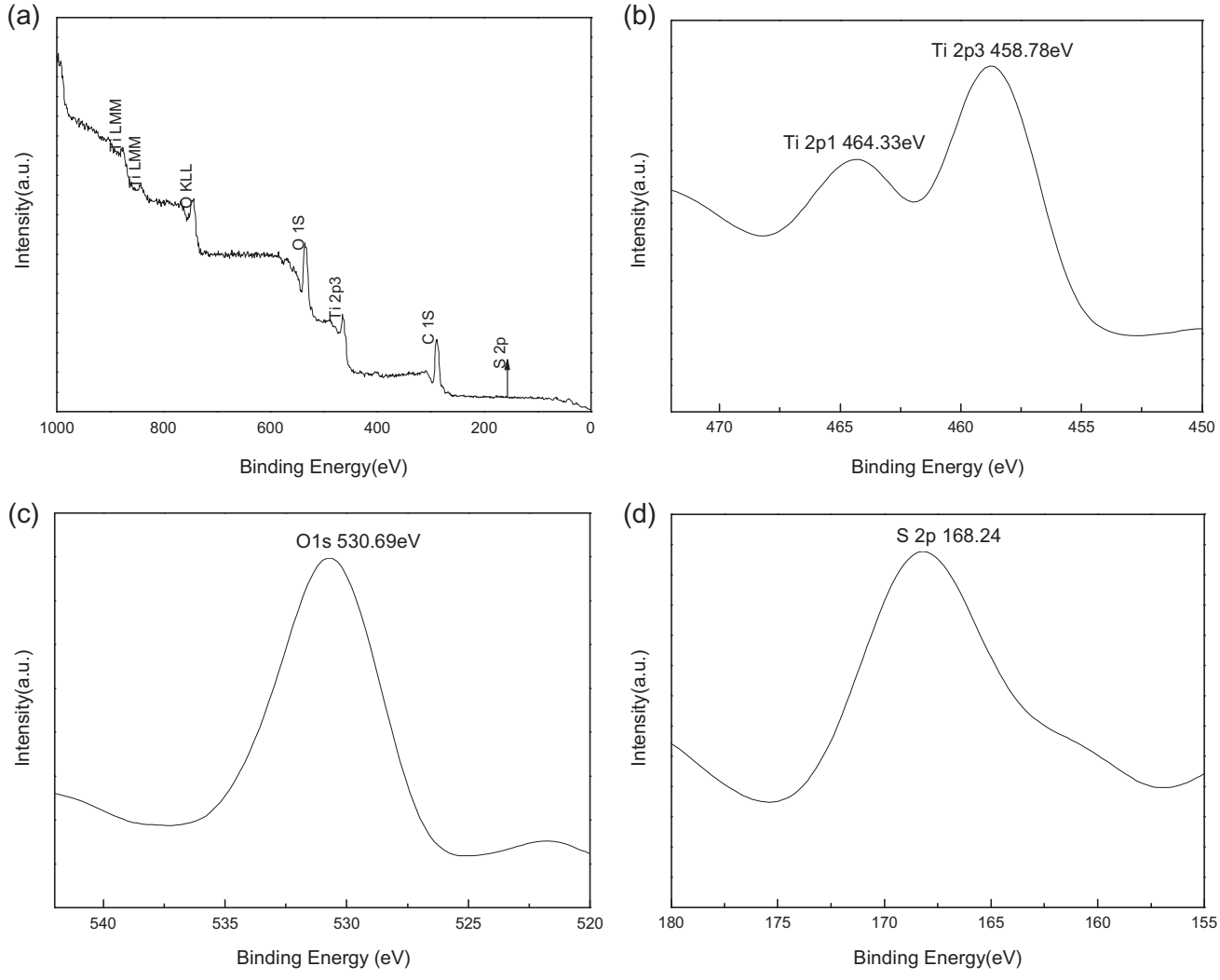


Fig. 8. The XPS spectra of (a) TS, (b) Ti 2p1 and Ti 2p3 of TS, (c) O 1s of TS, (d) S 2p of TS, (e) TNS, (f) Ti 2p1 and Ti 2p3 of TNS, (g) O 1s of TNS, (h) N 1s of TNS, and (i) S 2p of TNS.

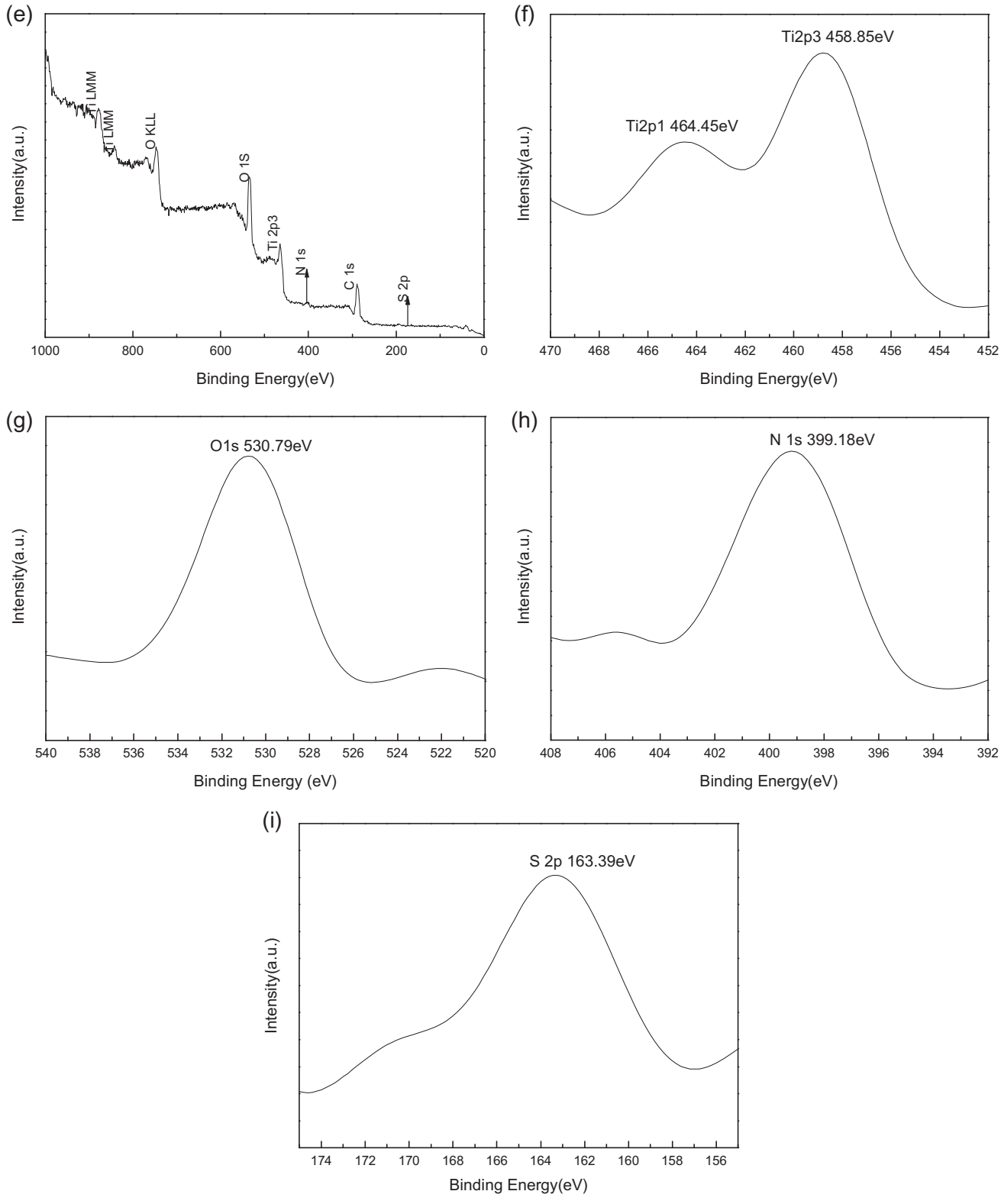


Fig. 8. (*Continued*)

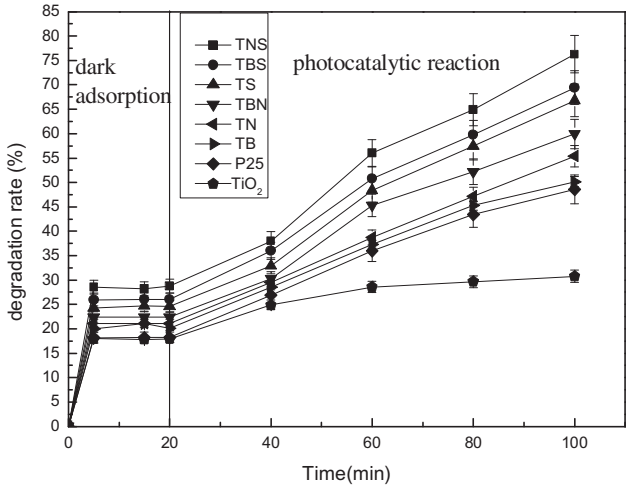


Fig. 9. The degradation rate of 10 mg/L salicylic acid with different photocatalysts.

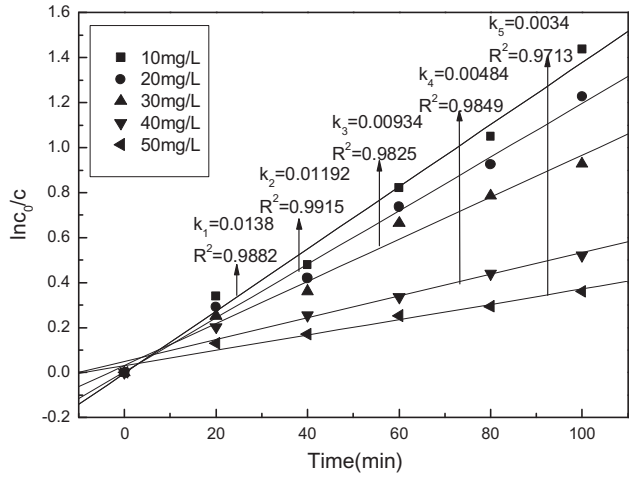


Fig. 11. The first-kinetic of TNS at different initial concentration salicylic acid.

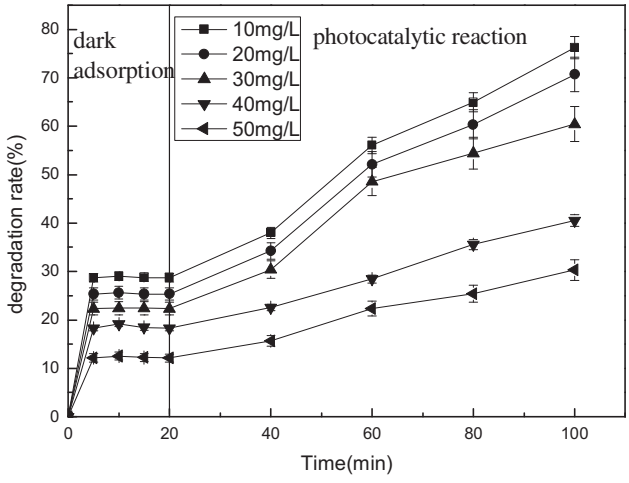


Fig. 10. The degradation influence of different initial concentration salicylic acid with TNS.

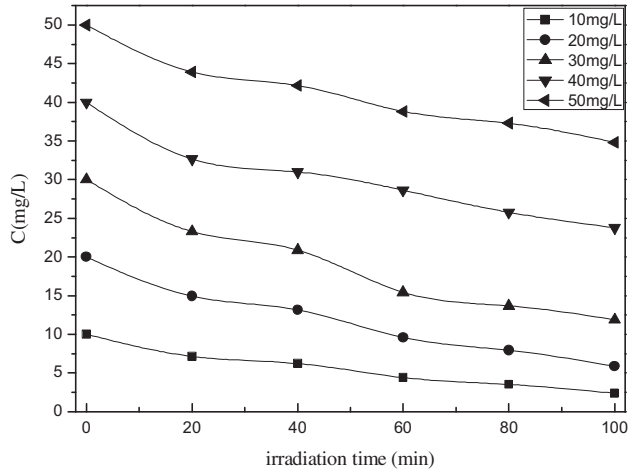


Fig. 12. The variation of salicylic acid for different initial concentrations.

0.0138 $S^{-1}$, and it is the largest than the other rate constant.

The experimental data can be rationalized in terms of the modified form of Langmuir–Hinshelwood kinetic treatment, which has already been successfully used to describe solid–liquid reactions [2]. In the Langmuir–Hinshelwood kinetics treatment of heterogeneous surface reactions, this treatment obeys to the assumptions that sorption of both the oxidant and the reductant is a rapid equilibrium process in both the forward and reverse directions. And the rate-determining step of the reaction involves both species present in a monolayer at the solid-liquid interface. The reaction rate ($r$) varies proportionally with the surface coverage ($\theta$) is given by formula (2):

$$r = -\frac{dC}{dt} = k_r\theta = \frac{k_r K_{eq} C}{1 + K_{eq} C} \quad (2)$$

where $k_r$ and $K_{eq}$ are the reaction rate constant and the equilibrium constant, and $C$ is the concentration of salicylic acid. The initial photocatalytic degradation rate ($r_0$) is observed to be a function of the initial concentration ($C_0$) of salicylic acid. A linear plot of $1/r_0$ vs. $1/C_0$ is obtained, that gives $k$ as the Langmuir–Hinshelwood

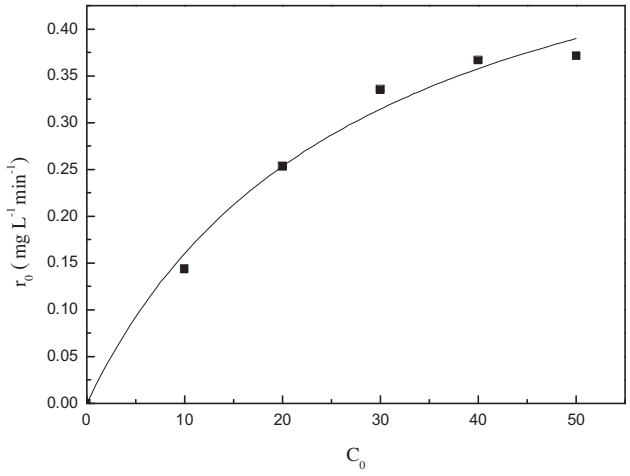


Fig. 13. The initial react rate ($r_0$) for initial concentration of salicylic acid.

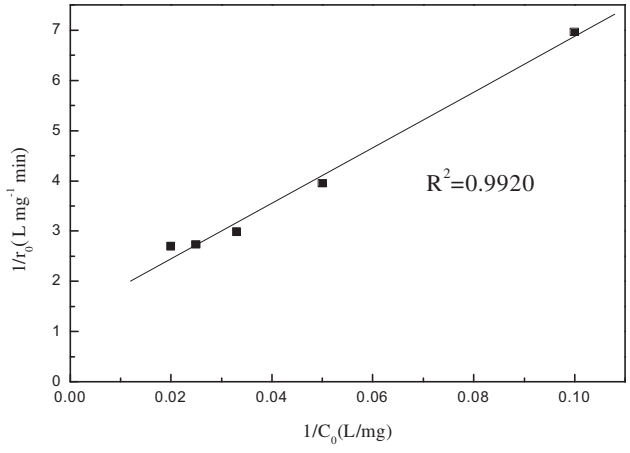


Fig. 14. Langmuir–Hinshelwood plots of the reciprocal of the initial reaction rate vs. the reciprocal of the initial concentration of salicylic acid.

rate constant and $K_{eq}$ as the Langmuir adsorption constant of the salicylic acid in the degradation reaction, and the formula could be changed to the formula (3).

$$r_0 = \frac{kK_{eq}C_0}{1 + K_{eq}C_0} \quad \text{or} \quad \frac{1}{r_0} = \frac{1}{kK_{eq}}\frac{1}{C_0} + \frac{1}{K_{eq}} \tag{3}$$

In order to find the effect of initial concentration on the initial react rate, more detailed analysis was fulfilled based on the kinetics of photocatalytic degradation reaction. Fig. 13 shows the variation of salicylic acid for different initial concentrations. As can be seen in Fig. 12, the initial slope increased with increasing initial concentration of salicylic acid, but maintained almost constant beyond a certain concentration. Fig. 13 describes the initial react rate ($r_0$) for initial concentration of salicylic acid. The steep rise of the rate at low levels of the salicylic acid and the subsequent mild variations is a typical behavior of Langmuir–Hinshelwood kinetics [29,30]. Fig. 14 represents plot of the reciprocal of the initial rate $r_0^{-1}$ vs. the reciprocal of the initial salicylic acid concentration $C_0^{-1}$ for degradation of salicylic acid. We can find from Fig. 14 that a good fitting of the model to the experimental data may be observed thus confirming the Langmuir–Hinshelwood nature of the photocatalytic degradation reaction mechanism.

## 4. Conclusions

In this work, we have prepared single-doped and co-doped $TiO_2$ using solvothermal synthesis via a simple way. From the characterization, results indicate that the morphology of TN and TNS are piled up by the highly intense uniform crystal. The images of TN and TNS at high magnification show many randomly oriented nanocrystallites with sizes 20–30 and 10–15 nm, respectively. The BET surface areas of TS and TNS are 97.82 and 140.72 $m^2/g$, respectively. It is confirmed that S as $S^{6+}$ incorporate into in the crystal lattice of the S–$TiO_2$, which may be the O–S–O–Ti–O linkages in the crystal lattice. It may be N and S as Ti–N–O or Ti–N–$O_2$ and $S^{2-}$ in the crystal lattice of the N&S co-doped $TiO_2$, respectively, which may be the S–Ti–N–O linkages in the crystal lattice. Photocatalytic activity was studied by degradation of salicylic acid under visible light. The photocatalytical activity of single-doped and co-doped $TiO_2$ were better than that of pure $TiO_2$ and p25. The highest degradation rate of salicylic acid could reach 76.25% with TNS photocatalyst in 120 min under visible light irradiation. And the kinetics of photocatalytic degradation obeyed first-order kinetic, which the rate constant value of degradation salicylic acid with TNS photocatalyst was 0.0138 $S^{-1}$.

## Acknowledgments

We gratefully acknowledge the financial support of the National Natural Science Foundation of China (No. 21207053), the Natural Science Foundation of Jiangsu Province (BK20130489), the Specialized Research Fund for the Doctoral Program of Higher Education (20113227110019), and China Postdoctoral Science Foundation (2011M500861, 2011M500869).

## References


[1] W.L. Guo, X.L. Liu, P.W. Huo, X. Gao, D. Wu, Z.Y. Lu, Y.S. Yan, Hydrothermal synthesis spherical $TiO_2$ and its photo-degradation property on salicylic acid, Appl. Surf. Sci. 258 (2012) 6891–6896.

[2] M.R. Hoffmann, S.T. Martin, W. Choi, D.W. Bahnemann, Environmental applications of semiconductor photocatalysis, Chem. Rev. 95 (1995) 69–96.

[3] B. Ohtani, Y. Ogawa, S.i. Nishimoto, Photocatalytic activity of amorphous-anatase mixture of titanium(IV) oxide particles suspended in aqueous solutions, J. Phys. Chem. B 101 (1997) 3746–3752.

[4] Y. Ishibai, J. Sato, T. Nishikawa, S. Miyagishi, Synthesis of visible-light active $TiO_2$ photocatalyst with Pt-modification: Role of $TiO_2$ substrate for high photocatalytic activity, Appl. Catal. B: Environ. 79 (2008) 117–121.

[5] T.Y Ma, J.L. Cao, G.S. Shao, X.J. Zhang, Z.Y. Yuan, Hierarchically structured squama-like cerium-doped titania: Synthesis, photoactivity, and catalytic CO oxidation, J. Phys. Chem. C 113 (2009) 16658–16667.

[6] R. Liu, Y. Ren, Y. Shi, F. Zhang, L. Zhang, B. Tu, D. Zhao, Controlled synthesis of ordered mesoporous C-$TiO_2$ nanocomposites with crystalline titania frameworks from organic-inorganic-amphiphilic coassembly, Chem. Mater. 20 (2008) 1140–1146.

[7] X. Lu, B. Tian, F. Chen, J. Zhang, Preparation of boron-doped $TiO_2$ films by autoclaved-sol method at low temperature and study on their photocatalytic activity, Thin Solid Films 519 (2010) 111–116.

[8] J. Xu, Y. Ao, D. Fu, C. Yuan, A simple route to synthesize highly crystalline N-doped $TiO_2$ particles under low temperature, J. Cryst. Growth 310 (2008) 4319–4324.

[9] J.H. Pan, X. Zhang, A.J. Du, D.D. Sun, J.O. Leckie, Self-etching reconstruction of hierarchically mesoporous F-$TiO_2$ hollow microspherical photocatalyst for concurrent membrane water purifications, J. Am. Chem. Soc. 130 (2008) 11256–11257.

[10] Y. Wang, J. Li, P. Peng, T. Lu, L. Wang, Preparation of S-$TiO_2$ photocatalyst and photodegradation of L-acid under visible light, Appl. Surf. Sci. 254 (2008) 5276–5280.

[11] X. Hong, Z. Wang, W. Cai, F. Lu, J. Zhang, Y. Yang, N. Ma, Y. Liu, Visible-light-activated nanoparticle photocatalyst of iodine-doped titanium dioxide, Chem. Mater. 17 (2005) 1548–1552.

[12] D. Li, W. Dong, S. Sun, Z. Shi, S. Feng, Photocatalytic degradation of acid chrome blue K with porphyrin-sensitized $TiO_2$ under visible light, J. Phys. Chem. C 112 (2008) 14878–14882.

[13] R. Asahi, T. Washizuka, N. Yoshino, K. Aoki, Y. Taga, Visible-light photocatalysis in nitrogen-doped titanium oxides, Science 293 (2001) 269–271.

[14] T. Ohno, M. Akiyoshi, T. Umebayashi, K. Asai, T. Mitsui, M. Matsumura, Preparation of S-doped $TiO_2$ photocatalysts and their photocatalytic activities under visible light, Appl. Catal., A 265 (2004) 115–121.

[15] T. Ohno, T. Mitsui, M. Matsumura, Photocatalytic activity of S-doped $TiO_2$ photocatalyst under visible light, Chem. Lett. 32 (2003) 364–365.

[16] T. Lindgren, J.M. Mwabora, E.D. Avendano Soto, J. Jonsson, A. Hoel, C.G. Graqvist, S.E. Lindquist, Photoelectrochemical and optical properties of nitrogen doped titanium dioxide films prepared by reactive DC magnetron sputtering, J. Phys. Chem. B 107 (2003) 5709–5716.

[17] G. Wu, J. Wen, J. Wang, D.F. Thomas, A.C. Chen, A facile approach to synthesize N and B co-doped $TiO_2$ nanomaterials with superior visible-light response, Mater. Lett. 64 (2010) 1728–1731.

[18] S. In, A. Orlov, R. Berg, F. Garcla, S. Pedrosa-Jimenez, M.S. Tikhov, D.S. Wright, R.M. Lambert, Effective visible light-activated B-doped and B, N-Co doped $TiO_2$ photocatalysts, J. Am. Chem. Soc. 129 (2007) 13790–13791.

[19] M. Sathish, R.P. Viswanath, C.S. Gopinath, N, S-Co-doped $TiO_2$ nanophotocatalyst: Synthesis, electronic structure and photocatalysis, J. Nanosci. Nanotechnol. 9 (2009) 423–432.

[20] S. Yin, K. Ihara, Y. Aita, M. Komatsu, T. Sato, Visible-light induced photocatalytic activity of $TiO_{2-x}$ Ay (A = N, S) prepared by precipitation route, J. Photochem. Photobio. A Chem. 179 (2006) 105–114.

[21] J. Yu, M. Zhou, B. Cheng, X. Zhao, Preparation, characterization and photocatalytic activity of in situ N, S-codoped $TiO_2$ powders, J. Mol. Catal. A: Chem. 246 (2006) 176–184.

[22] M. Pelaez, N.T. Nolan, S.C. Pillai, M.K. Seery, P. Falaras, A.G. Kontos, P.S.M. Dunlop, J.W.J. Hamilton, J.A. Byrne, K. O'Shea, M.H. Entezari, D.D. Dionysiou, A review on the visible light active titanium dioxide photocatalysts for environmental applications, Appl. Catal., B: Environ. 125 (2012) 331–349.

[23] L.S. Birks, H. Friedman, Particle size determination from X-ray line broadening, J. Appl. Phys. 17 (1946) 687–692.

[24] J. Virkutyte, S.R. Al-Abed, D.D. Dionysiou, Depletion of the protective aluminum hydroxide coating in $TiO_2$-based sunscreens by swimming pool water ingredients, Chem. Eng. J. 191 (2012) 95–103.

[25] T. Kubo, A. Nakahira, Local structure of $TiO_2$-derived nanotubes prepared by the hydrothermal process, J. Phys. Chem. C 112 (2008) 1658–1662.

[26] M. Sathish, B. Viswanathan, R.P. Viswanath, C.S. Gopinath, Synthesis, characterization, electronic structure, and photocatalytic activity of nitrogen-doped $TiO_2$ nanocatalyst, Chem. Mater. 17 (2005) 6349–6353.

[27] G. Balasubramanian, D.D. Dionysiou, M.T. Suidan, I. Baudin, J.M. Lâiné, Evaluating the activities of immobilized $TiO_2$ powder films for the photocatalytic degradation of organic contaminants in water, Appl. Catal., B: Environ. 47 (2004) 73–84.

[28] Y. Chen, D.D. Dionysiou, A comparative study on physicochemical properties and photocatalytic behavior of macroporous $TiO_2$-P25 composite films and macroporous $TiO_2$ films coated on stainless steel substrate, Appl. Catal., A 317 (2007) 129–137.

[29] S.B Kim, S.C Hong, Kinetic study for photocatalytic degradation of volatile organic compounds in air using thin film $TiO_2$ photocatalyst, Appl. Catal. B: Environ. 35 (2002) 305–315.

[30] T. Sauer, G.C. Neto, H.J. José, R.F.P.M. Moreira, Kinetics of photocatalytic degradation of reactive dyes in a $TiO_2$ slurry reactor, J. Photochem. Photobiol. A: Chem. 149 (2002) 147–153.